ELSEVIER

Contents lists available at ScienceDirect

Medical Engineering & Physics

journal homepage: www.elsevier.com/locate/medengphy



Carotid artery stenting simulation: From patient-specific images to finite element analysis

F. Auricchio^{a,c}, M. Conti^{a,b,*}, M. De Beule^b, G. De Santis^b, B. Verhegghe^b

- ^a Dipartimento di Meccanica Strutturale, Università degli Studi di Pavia, Pavia, Italy
- ^b IBiTech, Institute Biomedical Technology, Ghent University, Ghent, Belgium
- ^c CESNA Centro di Simulazione Numerica Avanzata IUSS, Pavia, Italy

ARTICLE INFO

Article history:
Received 26 June 2010
Received in revised form 8 October 2010
Accepted 10 October 2010

Keywords: Finite element analysis (FEA) Patient-specific model Carotid artery stenting (CAS)

ABSTRACT

The outcome of carotid artery stenting (CAS) depends on a proper selection of patients and devices, requiring dedicated tools able to relate the device features with the target vessel. In the present study, we use finite element analysis to evaluate the performance of three self-expanding stent designs (laser-cut open-cell, laser-cut closed-cell, braided closed-cell) in a carotid artery (CA). We define six stent models considering the three designs in different sizes and configurations (i.e. straight and tapered), evaluating the stress induced in the vessel wall, the lumen gain and the vessel straightening in a patient-specific CA model based on computed angiography tomography (CTA) images.

For the considered vascular anatomy and stents, the results suggest that: (i) the laser-cut closed-cell design provides a higher lumen gain; (ii) the impact of the stent configuration and of the stent oversizing is negligible with respect to the lumen gain and relevant with respect to the stress induced in the vessel wall; (iii) stent design, configuration and size have a limited impact on the vessel straightening. The presented numerical model represents a first step towards a quantitative assessment of the relation between a given carotid stent design and a given patient-specific CA anatomy.

 $\hbox{@ 2010 IPEM. }$ Published by Elsevier Ltd. All rights reserved.

1. Introduction

Atherosclerotic stenosis of the carotid artery (CA), narrowing the bifurcation neck, causes 20% of all ischemic strokes and transient ischemic attacks [1,2]. Carotid endarterectomy (CEA) is considered the gold standard for severe CA stenosis [3] but, recently, carotid artery stenting (CAS) is emerging as a safe and cost-effective alternative to CEA [4–6]. However, the widespread acceptance of CAS and its effectiveness compared to CEA is still a matter of debate, especially in case of symptomatic patients [7].

The clinical experts underline that the success of CAS is strongly dependent on the operator ability and should be supported by a proper selection of patients and devices [8]. Many dedicated CAS devices (e.g. stents, embolic protection devices (EPDs), guidewires, etc.) are available on a rapidly growing market, which on the one hand, is enlarging the available interventional options but, on the other hand, is complicating the standardization of the treatment strategy. Moreover, it is evident that CAS outcomes are essentially related to anatomic considerations [9].

These aspects indicate a significant need to develop dedicated tools for both procedure planning and device selection in order to relate the device features with the target vascular anatomy.

Although computational tools, as finite element analysis (FEA), are largely used to investigate several aspects of coronary stenting, such as the evaluation of interventional technique options [10] or the impact of plaque composition on vessel wall stress [11], few FEA studies are available on CAS [12–14]. In the present study, we use FEA to evaluate the performance of three self-expanding 1 stent designs in the CA. The study is organized as follows:

- we generate a patient-specific CA model based on DICOM images of computed tomography angiography (CTA);
- we generate six stent models considering three stent designs (laser-cut open-cell, laser-cut closed-cell, braided closed-cell) in different sizes and configurations (i.e. straight and tapered²);

^{*} Corresponding author at: Dipartimento di Meccanica Strutturale, Università di Pavia, Via Ferrata 1, 27100 Pavia, Italy. Tel.: +39 0382985980. E-mail address: michele.conti@unipv.it (M. Conti).

¹ With respect to deployment mechanics, stents can be classified as: (i) balloon-expandable (BX) and (ii) self-expanding (SX). BX stents are mounted on a balloon which is gradually inflated driving the stent deployment. SX stents are manufactured at the vessel diameter, then crimped and constrained in the delivery system; during the deployment the SX stent is gradually released from the catheter recovering the target diameter thanks to its mechanical properties [15].

² The distal diameter is smaller than the proximal one in order to set a conical shape to better take into account the diameter difference between the common carotid artery (CCA) and the internal carotid artery (ICA).

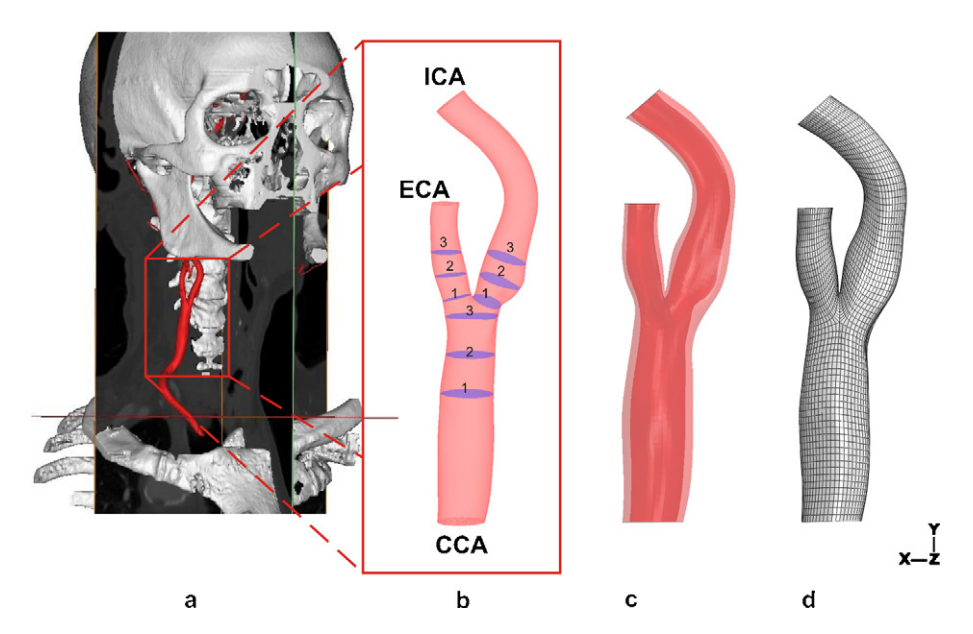


Fig. 1. Patient-specific CA model: (a) 3D reconstruction of cerebral vascular tree from CTA; (b) lumen of CA main branches (CCA: common carotid artery; ICA: internal carotid artery; ECA: external carotid artery); (c) CA lumen (dark red) and reconstructed outer vessel wall profile (light red); (d) hexahedral mesh. (For interpretation of the references to color in this figure legend, the reader is referred to the web version of the article.)

- for each stent model, we simulate the deployment in the CA model;
- we analyze the simulation results with respect to vessel stress, comparing also the pre- and post-stenting vessel geometry to evaluate the lumen gain and vessel straightening.

2. Materials and methods

Although CAS is a complex procedure which takes place in several steps, we focus on the stent implantation therefore the following parts are included in the simulations:

- a patient-specific CA model;
- the stent:
- the catheter.

The numerical analysis is clearly non-linear, involving large deformation and contact; consequently we use Abaqus/explicit as finite element solver (see Section 2.3).

In the following we describe the generation of the CA model, the generation of the stent models, the FEA settings and the postprocessing of the numerical results.

2.1. Patient-specific CA model

We process the DICOM CTA images of a stenosed carotid bifurcation of a 83 years-old male patient using Mimics v.13 (Materialise, Leuven, Belgium) to: (i) select the region of interest; (ii) compute the vessel centerline; (iii) remove secondary branches; (iv) generate an STL file defining the lumen profile (see Fig. 1(a)).

We use the open-source software pyFormex v.0.8 [16] to elaborate the obtained STL file to: (i) analyze the lumen of common carotid artery (CCA), external carotid artery (ECA) and internal carotid artery (ICA) (see Fig. 1(b) and Table 1); (ii) reconstruct the CA outer profile (see Fig. 1(c)); (iii) generate a high-quality, full hexahedral mesh with balanced resolution in each branch and minimal distortion for each element [17,18] (see Fig. 1(d)).

Since the medical images contain no information on the vessel wall thickness, we adopt a reconstruction strategy considering the wall thickness as a percentage (i.e., 30%) of the vessel radius in the

non-diseased region as suggested by values reported by Sommer et al. [19]. At the location of the stenosis, we reconstruct the outer wall interpolating the profile of the distal and proximal region by means of Bezier splines.

The vessel tissue is modeled as an isotropic hyperelastic material as proposed by Lally et al. [20,21]; despite the material parameters are calibrated on experimental data on human femoral artery and not on human CA, we believe that this model is appropriate for the purpose of the present study since it was successfully used for similar numerical analyses and based on accurate uni- and bi-axial tests on several tissue samples. The vessel density is assumed to be $1\,\mathrm{g/cm^3}$.

After a mesh sensitivity analysis (see Appendix A), we choose a final vessel mesh of 12,960 8-node linear brick, reduced integration elements with hourglass control (C3D8R).

We define ad hoc local cylindrical coordinate systems at the vessel ends to fix the corresponding nodes in the longitudinal and in the circumferential direction allowing consequently only radial displacements. Moreover, we assume no internal pressure on the vessel wall under the hypothesis that the geometry is based on measurements achieved at 80 mmHg.

2.2. Stent models

We consider three self-expanding stent designs: laser-cut open-cell, laser-cut closed-cell, braided closed-cell labeled, respec-

Table 1Geometrical measures of the branch sections highlighted in Fig. 1.

Branch	Sections	Mean radius \pm SD [mm]	Area [mm ²]
CCA	1	3.67 ± 0.12	41.56
	2	3.39 ± 0.08	35.52
	3	3.37 ± 0.39	33.62
ECA	1	2.11 ± 0.24	13.37
	2	2.19 ± 0.13	14.77
	3	2.14 ± 0.04	14.14
ICA	1	2.43 ± 0.27	17.71
	2	2.75 ± 0.26	23.24
	3	2.66 ± 0.17	21.91

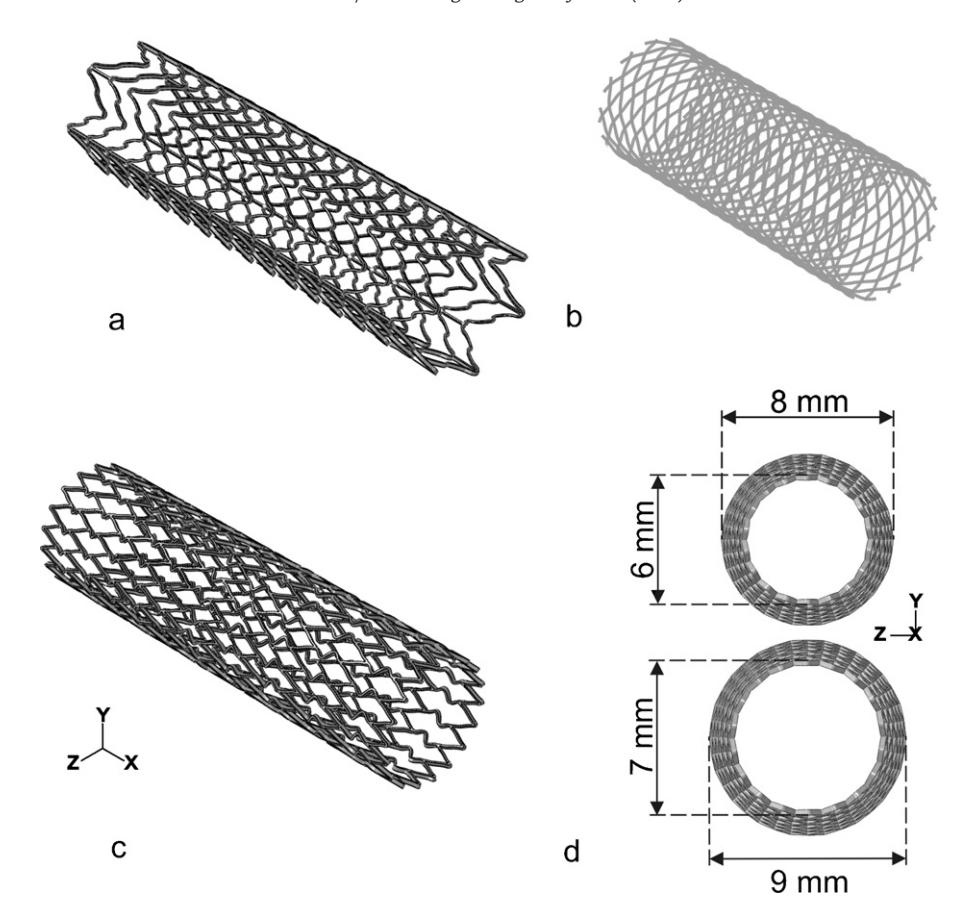


Fig. 2. Stent designs under investigation: (a) design A (straight configuration): laser-cut open-cell; (b) design C: braided closed-cell; (c) design B (straight configuration): laser-cut closed-cell; (d) design B (tapered configuration): model B2 (8–6 mm) and the oversized version model B2 (9–7 mm).

tively, indicated in the following as A, B, C and resembling three commercially available devices: the ACCULINK and the XACT (Abbott, IL, USA); the Wallstent (Boston Scientific Co., Natick, MA, USA). We define six stent models from the three designs as described in the following: the first two designs are considered both in straight configuration (labeled as stent A1 and B1) and in tapered configuration (labeled as stent A2 and B2); only one model (stent C1) of design C is considered since it is self-tapering; the sixth model (stent B3) is obtained oversizing stent B2.

In Fig. 2, the stent models A1, B1 and C1 are depicted to highlight the three different designs under investigation in their zero-stress state, while the details about size, configuration, number of nodes, number of elements for each model are reported in Table 2. We assume the same thickness of 0.24 mm for both designs A and B in order to focus the comparison mainly on the design features and not on the specific commercial device.

In the braided closed-cell stent model C, connectors elements (type JOIN) are introduced at the positions where there is physical contact between the crossing wires, in order to model the contact between these wires. The wire sliding is not allowed as each connector restrains the relative displacement between the tied nodes but allows the relative rotation [22,23].

While designs A and B are assumed to be manufactured in Nitinol, design C is assumed to be made in high strength Phynox, a cobalt–chromium alloy. The superelastic behavior of Nitinol is modeled using the Abaqus user material subroutine [24] originally proposed by Auricchio and Taylor [25,26] and based on the concept of generalized plasticity [27]. The adopted Nitinol constitutive parameters are obtained from literature [28] and considered identical for all stents; the density is assumed to be 6.7 g/cm³. Phynox is modeled as an elasto–plastic material having an elastic modulus of 206,000 MPa, Poisson's ratio of 0.33 and yield strength of 2450 MPa [29].

Table 2Geometrical and numerical details of the considered stent models.

Model label	A1	A2	B1	B2	В3	C1
Configuration	Straight	Tapered	Straight	Tapered	Tapered	Self-tapering
Cell type	Open-cell	Open-cell	Closed-cell	Closed-cell	Closed-cell	Closed-cell
Manufacturing	Laser-cut	Laser-cut	Laser-cut	Laser-cut	Laser-cut	Braided
Outer diameter [mm]	8	8-6	8	8-6	9–7	8
Strut thickness [mm]	0.24	0.24	0.24	0.24	0.24	0.12
Initial length [mm]	30	30	30	30	30	21
Number of nodes	159,230	159,230	171,720	171,720	171,720	7705
Number of elements	85,053	85,053	93,024	93,024	93,024	7680
Element type	C3D8R	C3D8R	C3D8R	C3D8R	C3D8R	B31
Material	Nitinol	Nitinol	Nitinol	Nitinol	Nitinol	Phynox

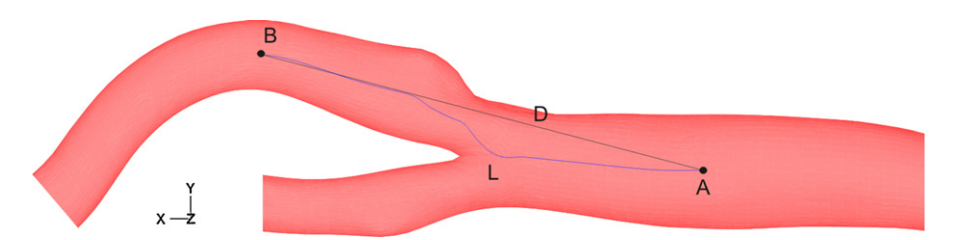


Fig. 3. Example of tortuosity computation (pre-stenting vessel): given the centerline, we quantify the vessel tortuosity computing the measure (L/D-1) for the stented CCA and ICA segment: L is the length of the centerline from the origin (point A) to the end of the stented region (point B) and D is the Euclidean distance between the two points; the tortuosity is therefore defined as the fractional increase in length of the tortuous vessel corresponding to a perfectly straight vessel.

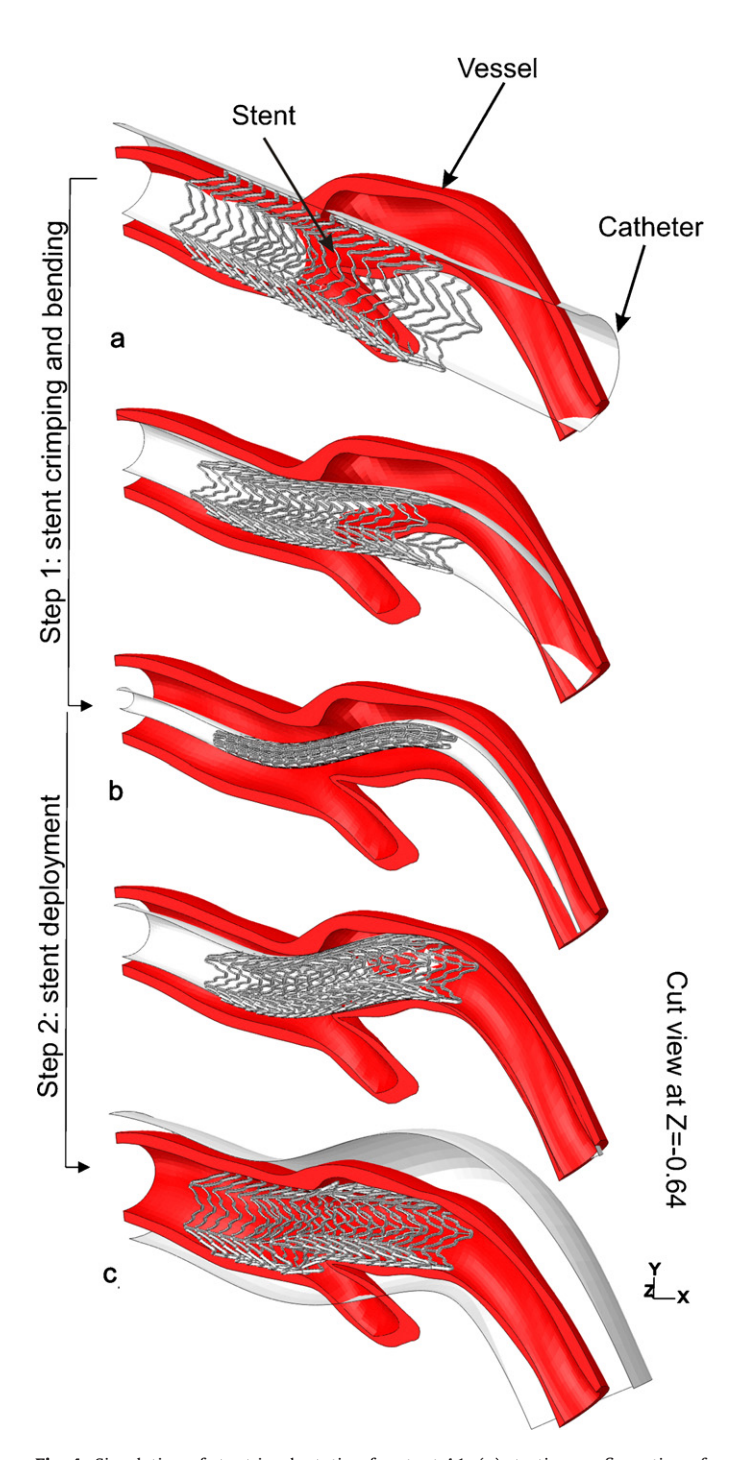


Fig. 4. Simulation of stent implantation for stent A1: (a) starting configuration of the FE model; (b) stent crimped in the delivery system; (c) stent deployed in the vessel.

2.3. FEA of CAS

The catheter is modeled as a rigid body defined by a surface obtained by sweeping a cylindrical section along the centerline of the vessel; we mesh it with 2760 three-dimensional, 4-node surface elements with reduced integration (SFM3D4R). In our simulation strategy, the stent deformation is imposed by the configuration change of the catheter set by displacement boundary conditions (BCs) on its nodes; the BCs are determined as the difference between a starting and final catheter configuration for each simulation step. In particular the simulation consists of two steps:

- stent crimping and bending: starting from a straight configuration the catheter is gradually bent and crimped accomplishing the vessel centerline and leading to the stent deformation; the contact between the stent and the vessel is deactivated in this step:
- 2. stent deployment: from the bent and crimped configuration, the catheter is re-enlarged and consequently the stent expands against the vessel wall; the contact between the stent and the vessel is activated in this step.

The numerical analysis is clearly non-linear, involving large deformations and contact; consequently we use Abaqus/explicit as finite element solver as this code provides a stable general contact

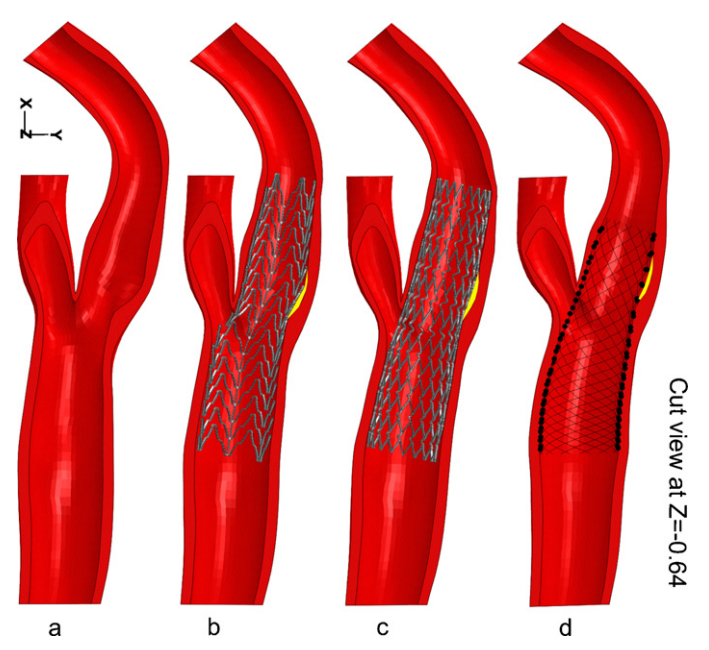


Fig. 5. (a) Pre-stenting carotid artery; (b) post-stenting carotid artery with stent A1; (c) post-stenting carotid artery with stent B1; (d) post-stenting carotid artery with stent C1. The gap between the stent and the vessel is highlighted in yellow. (For interpretation of the references to color in this figure legend, the reader is referred to the web version of the article.)

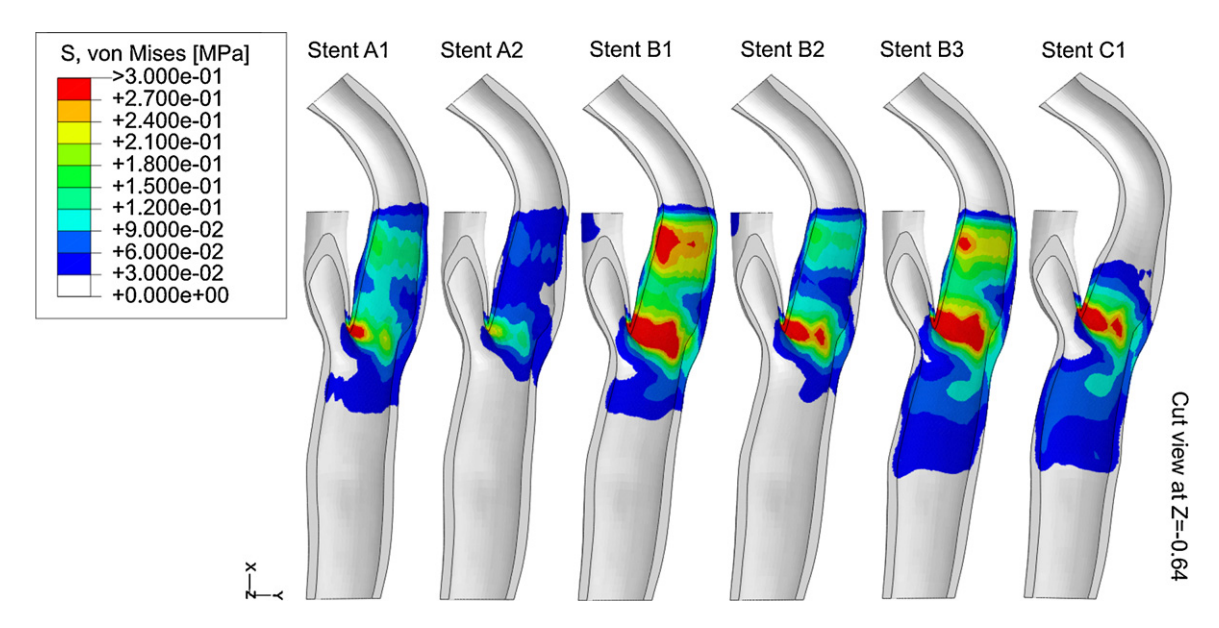


Fig. 6. Contour plot of von Mises stress distribution (S, von Mises) in the post-stenting carotid artery with respect to the different stent models.

algorithm. We use a mass scaling strategy to increase the minimum stable time increment, reducing the computational cost but, at the same time, we monitor the kinetic energy of all components during the simulation, since we consider the stent deployment as a quasi-static phenomenon where inertial forces are negligible (see Appendix A).

We use a general contact algorithm in order to handle the interactions between the parts: in particular, we set a frictionless contact between the stent and the catheter and a friction of 0.05 between the stent and the vessel surface [14].

2.4. Post-processing

We evaluate the impact of each stent model in the considered vessel focusing on the following aspects:

- von Mises stress distribution in the post-stenting vessel as a measure of potential injury induced by the stent apposition to the vessel wall. In fact, the supraphysiological stress state and the related vessel injury induced by the stent are important contributors for the complex process of restenosis [30]; consequently, the ideal stent should scaffold the vessel wall minimizing the induced stress:
- comparison of the pre- and post-stenting minimum lumen of the ICA as a measure of the lumen gain and of the stent capability to re-enlarge the stenosis;
- computation and comparison between the pre- and post-stenting vessel tortuosity as a measure of the vessel straightening induced by the stent insertion.

To neglect peak values of von Mises stress, due to local concentration, we consider the 99 percentile with respect to the pre-stenting vessel volume (i.e. only 1% of the volume has stress above this value). The pre- and post-stenting vessel tortuosity is measured as proposed by Thomas et al. [31] (see Fig. 3). The lumen calculation is performed using pyFormex and based on the inner surface of the vessel.

3. Results

Fig. 4 illustrates the vessel, stent and catheter configuration during the CAS simulation for stent A1 while Fig. 5 depicts the final

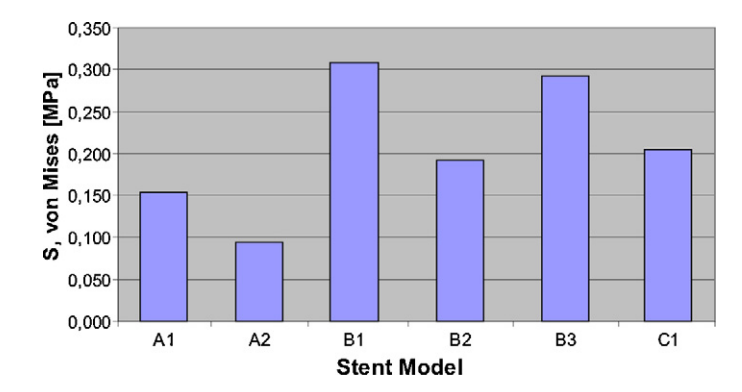


Fig. 7. 99 percentile of von Mises stress (S, von Mises) in the post-stenting carotid artery with respect to different stent models.

stent-vessel configuration for stent model A1, B1 and C1, allowing the qualitative evaluation of the stent apposition with respect to the three designs. All the analyzed models are not able to fully adapt to the lumen profile as highlighted by the gap between the stent and vessel at the beginning of the ICA bulb (slightly above the bifurcation); in case of stent A1, the simulation reproduces the so-called fish scaling³ effect [32] of the open-cell design A.

3.1. von Mises stress in the post-stenting vessel wall

Fig. 6 indicates that the maximum values of von Mises stress in the vessel wall are located near the bifurcation apex in all analyzed cases; this effect is related to the position of the stenosis which is also located at the beginning of the ICA bulb. The histograms depicted in Fig. 7 and the values reported in Table 3 indicate that:

- design A induces the lowest level of stress;
- design B induces the highest level of stress;
- the stress induced by braided closed-cell stent (C1) is similar to the stress induced by the tapered configuration of the laser-cut closed-cell design (B2);

³ When stent cells open on the concave surface of an angulated carotid bifurcation, they are prone to having prolapse and fish scaling on the open surface potentially resulting in intimal disruption.

Table 3 von Mises stress (99 percentile) for each stent model at the end of the simulation.

Stent model	A1	A2	B1	B2	В3	C1
von Mises stress [MPa]	0.1533	0.0940	0.3090	0.1916	0.2924	0.2048

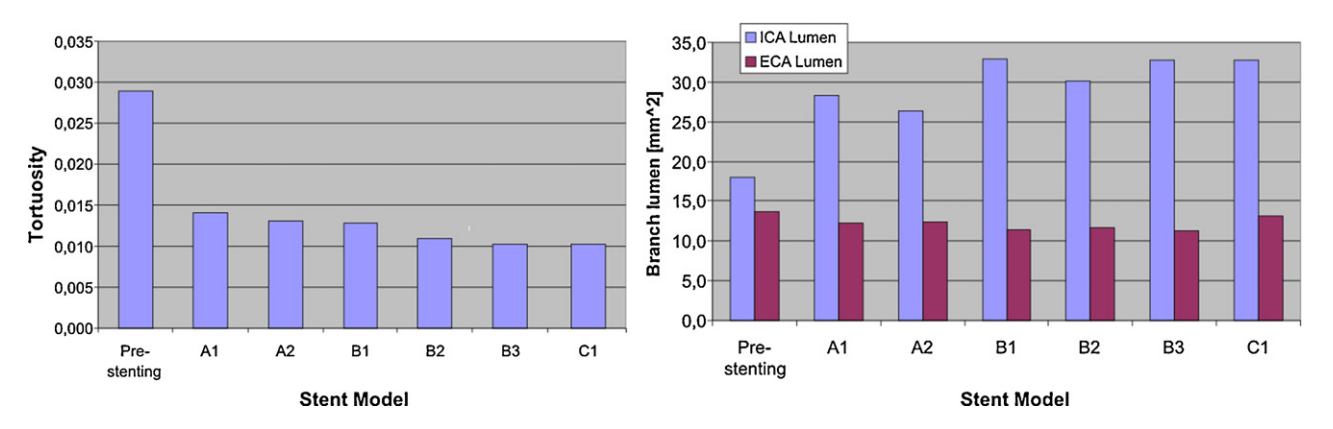


Fig. 8. Pre- and post-stenting tortuosity (on the left) and lumen of ICA and ECA (on the right).

Table 4Pre- and post-stenting branch lumen and tortuosity.

	Pre-stenting	Post-stenting					
Stent model		A1	A2	B1	B2	В3	C1
ICA lumen [mm ²]	18.0	28.3	26.4	32.9	30.1	32.8	32.73
ICA gain [%]	-	57.1	46.5	82.7	67.0	82.3	81.8
ECA lumen [mm ²]	13.6	12.3	12.4	11.4	11.8	11.3	13.11
Tortuosity	0.029	0.014	0.013	0.013	0.011	0.010	0.010

- for both designs A and B, the stress induced by the straight configuration is higher than the stress induced by the tapered configuration (stent A1 versus stent A2, +63%; stent B1 versus stent B2, +61%);
- in case of oversizing, i.e. stent B3 versus stent B2, the stress increases by 52%.

3.2. Lumen gain

The histograms depicted in Fig. 8 (on the right) and the values reported in Table 4 indicate that:

- all the stents provide a high ICA lumen gain (>45%) corresponding to a small reduction of the ECA lumen;
- for both designs A and B, the lumen gain provided by the straight configuration is higher than the lumen gain provided by the tapered configuration (stent A1 versus stent A2, +10%; stent B1 versus stent B2, +15%);
- in case of oversizing, i.e. stent B3 versus stent B2, the lumen gain increases by 15%.

3.3. Pre- and post-stenting tortuosity

The histograms depicted in Fig. 8 (on the left) and the values reported in Table 4 indicate that:

- all the stents straighten the vessel, reducing considerably the original stent tortuosity;
- stent design, configuration and size have a limited impact on the vessel straightening.

4. Limitations

We developed the CA model from in-vivo CTA images discarding a distinction of the plaque from the surrounding tissue, which would have an effect on the stress distribution in the vessel wall, lumen gain and degree of straightening; however, we believe that the comparative nature of this study makes the obtained results still valid. In future work, we plan to further improve the model including the plaque components (i.e. calcifications, fibrous tissue, or lipid core) assessed by in-vivo CTA [33,34] as proposed by a recent study [35]. Based on the NASCET method [36], the stenosis corresponds to a relative small vessel area reduction, i.e. 24%, which has no clinical indication for stenting [37]; future consideration of more severe degrees of stenosis would enforce the link between the presented simulations and the clinical practice.

We adopted an isotropic hyperelastic model for the vascular tissue as proposed by Lally et al. [20,21] who calibrated the material parameters on experimental data on human femoral artery; we believe that this model is appropriate for the purpose of the present study since it was successfully used for similar numerical analyses and based on accurate uni- and bi-axial tests on several tissue samples. Moreover, although some studies [38–40] provide already experimental data on human carotid artery, only recently Sommer et al. [19] have systematically determined the biomechanical behavior of human CCAs and ICAs; consequently we will use these data for further developments of the present study addressing anisotropic mechanical response of the CA tissue. Furthermore, we currently neglect axial pre-stretch, residual stresses and arterial blood pressure.

5. Conclusions

In the present study, we use FEA to evaluate the performance of three self-expanding stent designs, with different configurations and sizes, in a patient-specific CA model based on computed angiography tomography (CTA) images. We consider the stress induced to the vessel wall, the lumen gain and the vessel straightening as measures of stenting impact on the vessel anatomy. For the considered vascular anatomy and stents, the results suggest that: (i) the laser-cut closed-cell design provides a higher lumen gain; (ii) the impact of the stent configuration and of stent oversizing is negligible with respect to lumen gain and relevant with respect to the stress induced to the vessel wall; (iii) stent design, configuration and size have a limited impact on the vessel straightening.

Although the proposed numerical results refer to one specific vascular anatomy and three stent designs, we believe that the present study represents a first step towards a quantitative assessment of the relation between the complex mechanical features of a given carotid stent design and a given patient-specific CA anatomy, which could be useful for the procedure standardization. Clearly, due to the complexity of the system under investigation, the numerical results should be validated and embedded in a broader process accounting for clinical and biological considerations where the surgeon experience has a primary role.

Acknowledgments

This work is funded by PhD grant from MIUR (Ministero dell'Istruzione, dell'Università e della Ricerca, Italian Ministry of Education, University and Research).

The authors would acknowledge: Dr. R. Dore, Prof. A. Odero and Dr. S. Pirrelli of IRCCS Policlinico S. Matteo, Pavia, Italy, for support on medical aspects related to the present work; Dr. Taeymans of Ghent University Hospital, Ghent, Belgium, for the collection of stent samples; Eng. D. Van Loo of UGent University (UGCT), Ghent, Belgium, for micro-CT scanning of stent samples.

Appendix A

A.1. Mesh convergence analysis

We perform a mesh convergence analysis for the CA model discretization comparing the results of three different simulations (with three different vessel meshes) of CAS implant using stent B2 (see Table 5). We run all the simulation on 8 2.40 GHz cpus [41]. We focus on the following outputs obtained at the end of the simulation:

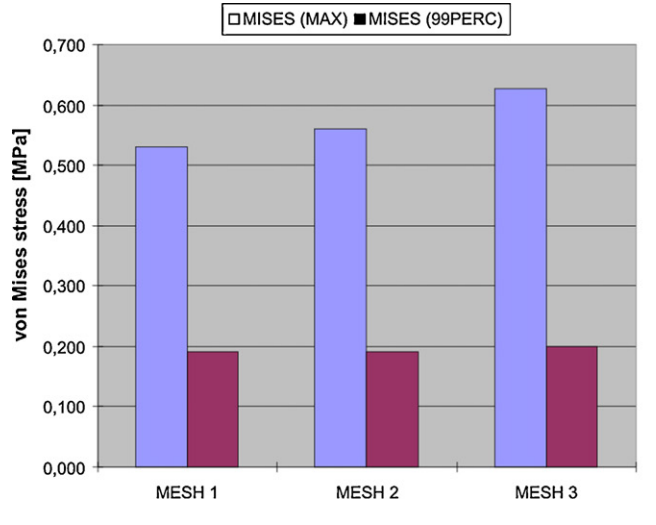


Table 5 Mesh convergence analysis.

Label	MESH 1	MESH 2	MESH 3
Number of nodes	17,564	31,100	60,595
Number of elements	12,960	23,040	48,000
Simulation time	22 h 41 min	24 h 12 min	27 h 57 min
U MAGNITUDE (MAX) [mm]	2.9457	3.0347	3.0295
MISES (MAX) [MPa]	0.530	0.5615	0.6273
MISES (99PERC) [MPa]	0.1916	0.1919	0.1990
LE MAX PRINC (MAX) [-]	0.3243	0.3368	0.3586
LE MAX PRINC (99PERC) [-]	0.2029	0.2025	0.2045

- displacement magnitude: we consider the maximum value U MAGNITUDE (MAX) – in the vessel node set;
- von Mises stress: we consider both the maximum value MISES (MAX) – in the vessel element set and 99 percentile – MISES (99PERC) – with respect to the pre-stenting vessel volume;
- maximum principal logarithmic strain: we consider both maximum value MISES (MAX) in the vessel element set and 99 percentile MISES (99PERC) with respect to the pre-stenting vessel volume.

The mesh convergence analysis (see Fig. 9) suggests that the mesh density increase has minor impact on the evaluated results; in particular only the maximum values of von Mises stress and strain (MISES (MAX), LE MAX PRINC (MAX)) are sensible to the mesh density; consequently, for the study purpose, we consider the respective 99 percentile values. Finally, we choose the MESH 1 since it has the lowest computational cost.

A.2. Kinetic-internal energy ratio

We simulate CAS performing a quasi-static analysis using Abaqus/explicit. In such analysis it is expedient to reduce the computational cost by either speeding up the simulation or by scaling the mass. In any case the kinetic energy (ALLKE) should be monitored to ensure that the ratio of kinetic energy to internal energy (ALLIE) does not get too large; we choose to use mass scaling adopting a threshold of 10% for energy ratio. We performed preliminary numerical tests (CAS implant using stent B2) to assess the impact of time step on such energy ratio and on computed values, varying the time step for step 2 from 0.03 s to 0.04 s. In Fig. 10, the ALLKE/ALLIE ratio for both cases is reported; two peaks of the energy ratio are present: (i) at beginning of the first step, due to the catheter/stent contact; (ii) at the beginning of the second step, due

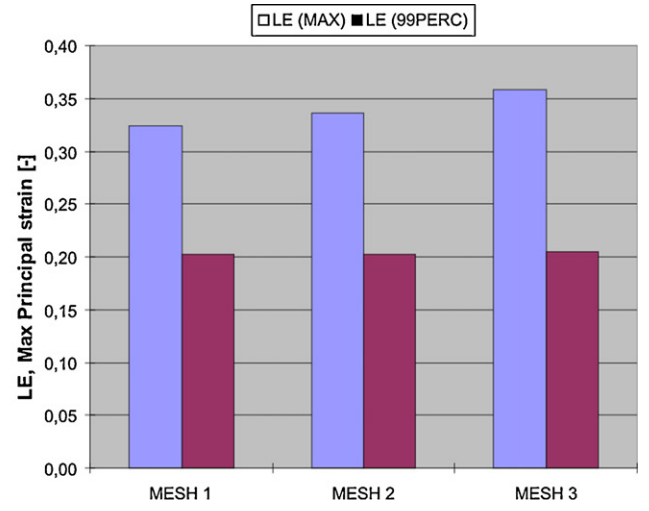


Fig. 9. Histograms depicting the von Mises and strain values as function of mesh density.

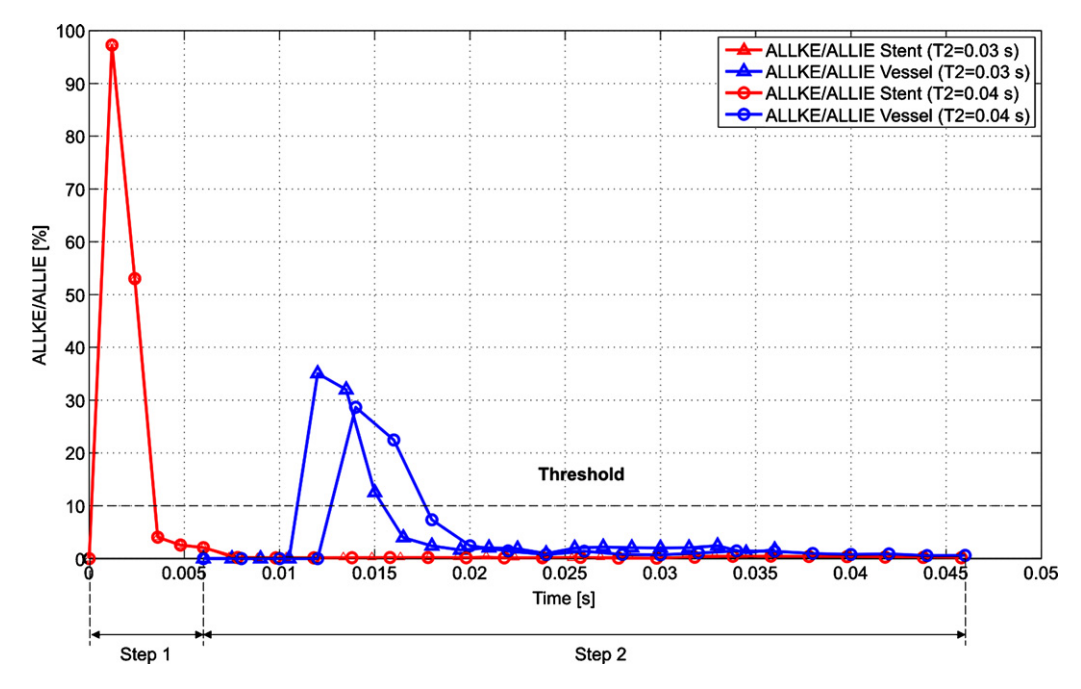


Fig. 10. ALLKE/ALLIE ratio for both stent and vessel during the simulation.

Table 6Impact of simulation time step on the computed values.

Time [s] (step 2)	0.03	0.04	Δ
Simulation time U MAGNITUDE (MAX) [mm] MISES (MAX) [MPa] MISES (99PERC) [MPa]	22 h 41 min 2.9457 0.530 0.1916	29 h 20 min 2.7 0.50 0.1812	-24% +8% +6% +5.7%
, ,,			

to the stent/vessel contact. For the goal of our study, we do not consider transient/intermediate values but only the results obtained at the end of the simulation, consequently we suppose that both peaks of ALLKE/ALLIE ratio have a limited impact on the proposed results as also demonstrated by the values reported in Table 6.

Conflict of interest statement

The authors report no conflicts of interest.

References

- [1] Chaturvedi S, Bruno A, Feasby T, Holloway R, Benavente O, Cohen S, et al. Carotid endarterectomy an evidence-based review: report of the Therapeutics and Technology Assessment Subcommittee of the American Academy of Neurology. Neurology 2005;65:794–801.
- [2] Cavatas. Endovascular versus surgical treatment in patients with carotid stenosis in the Carotid and Vertebral Artery Transluminal Angioplasty Study (CAVATAS): a randomised trial. Lancet 2001;357:1729–37.
- [3] Creager M, White C, Hiatt W, Criqui M, Josephs S, Alberts M, et al. Atherosclerotic peripheral vascular disease symposium II: executive summary. Circulation 2008;118:2811–25.
- [4] Forbes T. Preliminary results of carotid revascularization endarterectomy vs stenting trial (CREST). Journal of Vascular Surgery 2010;51:1300–1.
- [5] Liu Z, Shi Z, Wang Y, Chen B, Zhu T, Si Y, et al. Carotid artery stenting versus carotid endarterectomy: systematic review and meta-analysis. World Journal of Surgery 2009;33:586–96.
- [6] Brahmanandam S, Ding E, Conte M, Belkin M, Nguyen L. Clinical results of carotid artery stenting compared with carotid endarterectomy. Journal of Vascular Surgery 2008;47:343–9.
- [7] Paraskevas K, Mikhailidis D, Veith F. Mechanisms to explain the poor results of carotid artery stenting (CAS) in symptomatic patients to date and options to improve CAS outcomes. Journal of Vascular Surgery. doi:10.1016/j.jvs.2010.04.019.
- [8] Stockx L. Techniques in carotid artery stenting. European Journal of Radiology 2006;60:11–3.

- [9] Sayeed S, Stanziale S, Wholey M, Makaroun M. Angiographic lesion characteristics can predict adverse outcomes after carotid artery stenting. Journal of Vascular Surgery 2008;47:81–7.
- [10] Mortier P, De Beule M, Van Loo D, Verhegghe B, Verdonck P. Finite element analysis of side branch access during bifurcation stenting. Medical Engineering & Physics 2009;31:434–40.
- [11] Pericevic I, Lally C, Toner D, Kelly D. The influence of plaque composition on underlying arterial wall stress during stent expansion: the case for lesion-specific stents. Medical Engineering & Physics 2009;31:428–33.
- [12] Conti M, De Beule M, Mortier P, Van Loo D, Verdonck P, Vermassen F, et al. Nitinol embolic protection filters: design investigation by finite element analysis. Journal of Materials Engineering and Performance 2009;18:787–92.
- [13] Conti M, Auricchio F, De Beule M, Verhegghe B (06008) Numerical simulation of Nitinol peripheral stents: from laser-cutting to deployment in a patient specific anatomy. In: Proceedings of ESOMAT 2009. 2009., doi:10.1051/esomat/200906008.
- [14] Wu W, Qi M, Liu X, Yang D, Wang W. Delivery and release of nitinol stent in carotid artery and their interactions: a finite element analysis. Journal of Biomechanics 2007;40:3034–40.
- [15] Duerig T, Wholey M. A comparison of balloon- and self-expanding stents. Minimally Invasive Therapy and Allied Technologies 2002;11:173–8.
- [16] pyFormex. pyformex a tool for generating, manipulating and operating on large geometrical models of 3d structures by sequences of mathematical transformations. http://pyformex.berlios.de/ [accessed 15.06.10].
- [17] De Santis G, Mortier P, De Beule M, Segers P, Verdonck P, Verhegghe B. Patient-specific computational fluid dynamics: structured mesh generation from coronary angiography. Medical and Biological Engineering and Computing 2010;48:371–80.
- [18] De Santis G, De Beule M, Segers P, Verdock P, Verhegghe B. Patient-specific computational hemodynamics: generation of structured and conformal hexahedral meshes from triangulated surfaces of vascular bifurcations. Computer Methods in Biomechanics and Biomedical Engineering, in press.
- [19] Sommer G, Regitnig P, Koltringer L, Holzapfel G. Biaxial mechanical properties of intact and layer-dissected human carotid arteries at physiological and supraphysiological loadings. American Journal of Physiology: Heart and Circulatory Physiology 2009;298:H898–912.
- [20] Lally C, Dolan F, Prendergast P. Cardiovascular stent design and vessel stresses: a finite element analysis. Journal of Biomechanics 2005;38:1574–81.
- [21] Prendergast P, Lally C, Daly S, Reid A, Lee T, Quinn D, et al. Analysis of prolapse in cardiovascular stents: a constitutive equation for vascular tissue and finite-element modelling. Journal of Biomechanical Engineering 2003;125: 693-9.
- [22] De Beule M. Finite element stent design. PhD Thesis. Belgium: Ghent University; 2008.
- [23] De Beule M, Van Cauter S, Mortier P, Van Loo D, Van Impe R, Verdonck P, et al. Virtual stent optimization of self-expandable braided wire stents. Medical Engineering & Physics 2009;31:448–53.
- [24] Rebelo N, Walker N, Foadian H. Simulation of implantable stents. In: Abaqus user's conference, vol. 143. 2001. p. 421–34.
- 25] Auricchio F, Taylor R. Shape-memory alloys: macromodeling and numerical simulations of the superelastic behavior. Computer Methods in Applied Mechanics and Engineering 1997;146:281–312.

- [26] Auricchio F, Taylor R. Shape-memory alloys: modeling and numerical simulations of the finite-strain superelastic behavior. Computer Methods in Applied Mechanics and Engineering 1996;143:175–94.
- [27] Lubliner J, Auricchio F. Generalized plasticity and shape memory alloy. International Journal of Solids and Structures 1996;33:991–1003.
- [28] Kleinstreuer C, Li Z, Basciano C, Seelecke S, Farber M. Computational mechanics of Nitinol stent grafts. Journal of Biomechanics 2008;41:2370–8.
- [29] Clerc O, Jedwab M, Mayer D, Thompson P, Stinson J. Assessment of wrought ASTM F1058 cobalt alloy properties for permanent surgical implants. Journal of Biomedical Materials Research 1997;38:229–34.
- [30] Edelman E, Rogers C. Pathobiologic response to stenting. American Journal of Cardiology 1998;81:4E–6E.
- [31] Thomas J, Antiga L, Che S, Milner J, Hangan Steinman D, Spence J, et al. Variation in the carotid bifurcation geometry of young versus older adults: implications for geometric risk of atherosclerosis. Stroke 2005;36:2450–6.
- [32] Wholey M, Finol E. Designing the ideal stent. Endovascular Today 2007;6:25–34.
- [33] de Weert T, Ouhlous M, Meijering E, Zondervan P, Hendriks J, van Sambeek M, et al. In vivo characterization and quantification of atherosclerotic carotid plaque with components with multidetector computed tomography and histopathological correlation. Arteriosclerosis Thrombosis and Vascular Biology 2006;26:2366–72.
- [34] de Weert T, Ouhlous M, Zondervan P, Hendriks J, Dippel D, Van Sambeek M, et al. In vitro characterization of atherosclerotic carotid plaque with multidetector

- computed tomography and histopathological correlation. European Radiology 2005:1906–14.
- [35] Creane A, Maher E, Sultan S, Hynes N, Kelly D, Lally C. Finite element modelling of diseased carotid bifurcations generated from in vivo computerised tomographic angiography. Computers in Biology and Medicine 2010;40: 419–29
- [36] Albers G, Chang Y, Golby A. Detection of carotid stenosis: from NASCET results to clinical practice. Stroke 1995;26:1325–8.
- [37] Bates E. ACCF/SCAI/SVMB/SIR/ASITN 2007 clinical expert consensus document on carotid stenting. Journal of the American College of Cardiology 2007;49:126–70.
- [38] Stemper B, Yoganandan N, Pintar F. Methodology to study intimal failure mechanics in human internal carotid arteries. Journal of Biomechanics 2005;38:2491-6.
- [39] Tang D, Yang C, Kobayashi S, Ku N. Effect of a lipid pool on stress/strain distributions in stenotic arteries: 3-D fluid-structure interactions (FSI) models. Journal of Biomechanical Engineering 2004;126:363-70.
- [40] Delfino A, Stergiopulos N, Moore J, Meister J. Residual strain effects in the stress field in a thick wall finite element model of the human carotid bifurcation. Journal of Biomechanics 1997;30:777–86.
- [41] Bumper-cluster. A low cost/high performance linux cluster dedicated to computational mechanics. http://bumps.ugent.be/bumper/; 2009 [accessed 15.06.10].